Int. J. Nanoelectronics and Materials **6** (2013) 73-86

On the application of positron spectroscopy to heteronanostrutures

N. Yu. Arutyunov[1,*], Nadir Sekkal[2,3,4,5,#], H. Aourag[6]

[1] *Institute of Ionic-Plasma and Laser Technologies (Institute of Electronics), Tashkent 700187, Uzbekistan.*
[2] *Département de Physique-Chimie, Ecole Normale Supérieure de l'Enseignement Technologique, BP 1523, EL M'Naouer, 31000 Oran, Algeria.*
[3] *Laboratoire de Caractérisation et Simulation des Composants et Circuits électroniques (CaSiCCe), ENSET-Oran, BP 1523 EL M'Naouer, Oran 31000, Algeria.*
[4] *Laboratoire de Microphysique et de Nanophysique (LaMiN), ENSET-Oran, BP 1523 EL M'Naouer, Oran 31000, Algeria.*
[5] *Physia-Laboratory, BP 47 (RP), 22000 Sidi Bel Abbès, Algeria.*
[6] *Laboratoire d'Etude et de Prédiction de Matériaux, URMER, Université de Tlemcen, 13000 Tlemcen, Algeria.*

Received 4 May 2012; Revised 18 Sep. 2012; Accepted 3 Dec. 2012

Abstract

The band structure calculations have been performed for the defect-free GaAs-AlAs superlattice and the electron-positron momentum density distributions have been computed. The comparison of data of calculations with the experimental ones obtained for GaAs and AlAs constituent materials by measuring the angular correlation of the annihilation radiation (ACAR) demonstrates good agreement. The possibility of a confinement of positron in the superlattice is predicted. The elemental specificity of the atomic environment of positron is shown to determine the electron-positron momentum distribution for a confined positron in GaAs-AlAs superlattice. In the high-momentum region this distribution is affected by the positron annihilation on the electrons in the shells of Ga^{3+} and Al^{3+} ion cores. The change of the positron confined state to the trapped one is considered as an example for the vacancy-type defects present in GaAs constituent material. In this connection the non-destructive characterization of the heterostructures and superlattices by means of the positron self-seeking microprobe is shortly discussed.

Keywords: Superlattices, Characterization, Positron spectroscopy, Positron-electron annihilation, ACAR; DBAR.
PACS: 78.70.Bj, 73.40.Kp, 71.60.+z.

*) For correspondence, E-mail: n_arutyunov@yahoo.com

1. Introduction

Among different applications of the positron annihilation spectroscopy the investigations of the free volume of the defects of a vacancy type are the most wide-spread ones [1, 2]. The electron density around the positron, on the whole, characterizes the volume where it is localized as well as the chemical nature of the ion cores surrounding the positron when it annihilates in the defect of a vacancy type in the diamond-like semiconductors (as an example, see the data available for the point group-V-impurity vacancy complexes in the oxygen-lean germanium subjected to the irradiation with gamma rays of Co-60 [3-5]).

However, extremely high sensitivity of the positron to the areas in semiconductors containing negative effective charges manifests itself even in case the matter does not concern the defects of a vacancy type. The partial localization of positron in the field of the negative effective charge results in a selective annihilation of the positron with the core electrons surrounding the annihilation site. As the wave functions of the core electrons to a great extent retain their atomic character one can determine the chemical nature of the ion cores surrounding the positron [6]. The effect of the partial localization of positron has been studied for a number of years allowing one to come to a certain conclusions concerning configurational features of various oxygen-related point defects in silicon including the oxygen-related precipitates of a nano-scale size which are produced in the material by the heat treatment [7-9].

Similar effect of the positron localization unrelated to the positron trapping by defects of a vacancy type and to be considered as the *positron confinement* was found for so-called defect-"free" Cu precipitates produced by thermal aging in deluted Fe-Cu alloys [10]. Later on the positron confinement has been considered in a number of works [11-21]. On the whole, it has been established that the areas having in solids a characteristic size of a nano-cluster may create a potential well in which the positron is spatially confined in three dimensions [15].

The effect of the positron confinement by the quantum wells in GaAs-AlAs superlattice and related materials has recently been predicted in [22, 23]. It was found that the thermalized positron being partially localized is simultaneously confined in the region (s) which was shown to form (for the lack of a better term) the *positron superlattice.* It will be noted that GaAs-AlAs is capable of confining the positron similar, in many respects, to the effects of confinement described for both the nano-metric precipitates and the polar structures [24]. Further studying of the confinement has revealed the polarization of the positron in the field of the interfaces of heterostructures of the group-III nitrides GaN-AlN and GaN-InN which has clearly been seen in the predicted momentum distributions of the annihilating electron-positron pairs as the changes in them relative to the constituent bulk materials AlN, GaN, and InN [25].

It will be noted that the positron probing of the constituent materials by DBAR technique has been used for investigating defects in the layered superlattice-like structure of α-Si and SiO_2 materials on the substrate of Si single crystal and, presumably, some evidence of a confined positron state has been obtained [26]. On the contrary, the presence of the vacancy-impurity complexes in the structures of such type was established to create a localized state involving the impurity atoms of nitrogen as a result of the annealing process [26-28].

In the present paper, we show that the primary confinement of positron in the superlattice results in an elementally specific emission of the annihilation 2γ -quanta whose momentum distribution reflects a certain chemical nature of atoms at the annihilation site. In order to estimate the sensitivity and limitations of calculations based on a *modified* advanced scheme of empirical pseudopotential method, we have chosen GaAs-AlAs superlattice

because its constituent parts, GaAs and AlAs materials, have close densities of the bonding electrons. The most precise and informative positron annihilation technique, namely, ACAR spectroscopy, has been used as a basis for analyzing the emitted annihilation radiation including elementally specific components [29]. Special attention is given to the constituent materials of GaAs-AlAs superlattice in order to verify the predictions made with regard to the positron-containing quantum wells. The change of the positron confinement to the trapping of positron by a vacancy defects is shortly discussed for GaAs sublattice in order that to show a probable effects to be observed in ACAR spectra in case the emission of the annihilation radiation occurs from the positron trapped state

2. Experimental

The long-slit scheme of the installation possessing the angular resolution ~ 0.9 mrad (1 milliradian = $10^{-3}\ m_0c \approx 0.137\ a.u. \approx 0.057°$) has been used for measuring the ACAR spectra at room temperature (for more details see [3] and references therein). Thus, the precision of studies of the electron-positron momentum densities was, approximately, higher by a factor of ~ 5 compared to best available CDBAR techniques. Comparatively high angular resolution of the ACAR spectrometer has turned out to be crucial for correct comparing very close electron-positron momentum densities of the valence bands which are characteristic of AlAs and GaAs diamond-like semiconductors (see Sec. 4 for more detail).

We shall give only a short account of the samples of GaAs and AlAs materials which have been selected *ad hoc*. Single crystals *n*-GaAs<Si>, n~10^{17} cm^{-3}, oriented along [111], [100], and [110] crystallographic direction, were subjected to special treatment including the annealing of the samples in order to minimize the concentration of possible vacancy-type defects including *EL*2 arsenic antisites. On the contrary, as-grown material containing rather high concentration (typical value ~ 10^{16} – 10^{17} cm^{-3}) of the vacancy-type point defects was used for demonstrating their role in forming those electron-positron momentum distributions which are related to the positron trapping process.

The samples of AlAs were oriented along [111], [110] and [100] crystallographic directions in the process of recording of ACAR spectra, and special precautionary anti-corrosion measures were undertaken. These samples of AlAs and GaAs single crystals were used for determining the difference between both ACAR spectra and corresponding electron-positron momentum density distributions; then the comparison of experimental and calculated data has been performed.

3. Theory

In the present work the theoretical framework used earlier in [22, 23] has been applied. For determining the electronic states of both GaAs and AlAs bulk materials, we have used the empirical pseudopotential method (EPM) [30] which is known to omit determining properties of the electron states in the ion core region of the crystal. This method can be easily improved by applying the screened, spherical pseudopotentials that can be obtained using local density approximation (LDA). Then the latter is known to be adjusted for fitting with the measured band energies when keeping LDA quality wavefunctions [31]. At this stage of the comparative analysis of the results available we do not consider the comparison of the data obtained for the positron annihilation in the region of the ion cores in the crystal lattices of GaAs and AlAs. Thus, we use the local pseudopotentials for obtaining both the bulk bonding states and the superlattice positron states. Starting from the data available on the probability of the positron penetration into the

ion core region in solids we have good reasons to believe that this simplification is quite reasonable as a first approximation for the materials under study [29]. For simplicity, the spin-orbital interaction is not taken into account.

Once the parameters of the electron structure are obtained one may determine the positron states using the independent particle model (IPM) [32, 33]. This method is rather accurate for GaAs and AlAs semiconductors in which the enhancement of the positron annihilation rate is known and corresponding amendments related to the enhancement factor of the positron annihilation rate in the relatively dense ($r_s \approx 2 \;\; a.u$) electron Fermi gas are small and may, thus, be neglected. It is especially justifiable in case the matter concerns the electron-positron momentum density distribution; this conclusion is in agreement with the one formulated previously for various materials, in particular, for both diamond-like semiconductors [29] and organic conductors TTF-TCNQ [34]. In its turn, it means that one can avoid considerable inaccuracies in the final numeral results obtained for the electron-positron momentum density distributions.

Though the IPM approximation does not take into account the electron-positron interaction, nevertheless, this approach is qualitatively justifiable for the electron Fermi gas of a relatively high density (n) whose magnitude is equal to $r_s = \left(3/4\pi\, n\right)^{1/3} \approx 2\ a.u.$; this is not the case for relatively much lower electron densities to be characterized by r_s magnitudes over the range ~ 4 ÷ 6 *a.u.* which are characteristic of, e.g., the alkali metals (for more detail see, e.g. [35, 36]). Indeed, the local density approximation (LDA), which takes into account the screening electron cloud around the positron as well as generalized gradient approximation (GGA) connecting IPM and LDA, - these three ways of calculations are known to result in close electron-positron momentum distributions for a majority of solids (and even, in particular, for organic conductor TTF-TCNQ [34]). For diamond –like semiconductors the magnitudes r_s calculated by IPM, LDA and GGA are close to each other, too, thought the calculations based on IPM result in small (but marked) deviations from the data obtained by GGA [36]. At last, the momentum density distribution of the annihilation radiation is calculated by generalized formula:

$$\Gamma_{total}(\vec{p}) = \sum_n \Gamma_n(\vec{p}) \tag{1}$$

where

$$\Gamma_n(\vec{p}) = const \sum_{\vec{k}} \left| \int \exp(-i.\vec{p}.\vec{r}) \left(\Psi_p(n=1,\vec{k}=\Gamma,\vec{r}) \;\; \Psi_e(n,\vec{k},\vec{r}).d\vec{r} \right) \right|^2 \tag{2}$$

Here Ψ_p and Ψ_n are the wavefunctions of electrons and positrons respectively, n is the index of the electron band, $\vec{k}$ is the wave vector in the Brillouin zone of the bulk, $\vec{p}$ is the momentum of two annihilation photons, and $\Gamma_n(\vec{p})$ is the partial momentum density for the n^{th} band. The summation in Eq. (2) runs over all occupied electron states (i.e.; all valence states).

For the superlattice system, we have adopted the more advanced pseudopotential method of Jaros et al (PMJ) [37] which easily involves LDA calculated screened spherical pseudopotentials. The PMJ method allows one to treat adequately unstrained [37, 38], strained [39-41] and more complicated structures including defects [42-45]. PMJ has well been established for many years in the study of semiconductor superlattices, it expands wavefunction of the heterostructure on a set of wavefunctions formed on the basis of the

ones for the bulk of constituent materials. Its framework makes it possible a direct involvement of the symmetry of the supercells under study in the calculations; the method also makes it clear the link between the bulk states and those of their superlattice. PMJ satisfies the basic demands of our purpose since we are interested in the comparison of the numeral data obtained for the superlattice with the ones available for its bulk constituents. Just as for the bulk calculations, the ion core states are also omitted in the consideration and then only local pseudopotentials are used instead of the screened spherical pseudopotentials derived from LDA. On the other hand, only the PMJ version for the "ideal" case is needed. Polarization which has been recently found to localize the positron wavefunction at the interfaces [25] is not considered here. Below we are summarizing the general aspects of the method; complete details for the implementation of the calculation can be found elsewhere [38].

Finally, the momentum density distribution of the annihilation radiation for superlattices is calculated using the same formulas (1) and (2) which hold for both bulk materials and their superlattice. The only difference is that both $(n, \vec{k})$ and the wavefunctions in this case are all related to the superlattice.

4. Results

Of special interest is the total distribution of the electron-positron momentum density in so far as it is this distribution that is detected by ACAR measurements. The latter is obtained using formula (1) by superimposing all functions of partial electron-positron momentum densities as defined by formula (2). It is important to note that *there is observed a saddle-like shape* of the total distribution of the electron-positron momentum density for [011] direction which is characteristic of the momentum density distribution for tetrahedral crystal lattices (Fig. 1 in Ref. [23]). For [100] crystallographic direction of the materials under study there have been obtained similar electron positron momentum distributions possessing of their own anisotropic features; for not to encumber the paper with unnecessary details we do not present corresponding figures.

We would like to draw the reader's attention to two facts of behaviour of the total distribution of the electron-positron momentum density in GaAs/AlAs superlattice: (*i*) the minimum observed at $p_z = 0$ *a.u.* as well as (*ii*) rather abrupt change of the derivative near to the value $p_z \sim 0.9$ *a.u.* (or, using more customary units, p_z is equal to $\approx 6.81 \times 10^{-3}$ [m_0c]); on the whole, this value is close to the Fermi momentum of the bonding electrons in the single crystals of GaAs and AlAs as well as in GaAs/AlAs superlattice (see Fig. 1). These peculiarities, (*i*) and (*ii*), are a fingerprint reflecting the symmetry of the diamond-like crystal lattice. Also, these data indicate *reliability* and correctness of the whole scheme of calculations described above in Sec. 3 inasmuch us these calculated data follow the experimental ones (see below in more detail as well as Fig. 1).

In this connection it is important to emphasize observing a step-like drop over the range of momenta from ~ 3.5 to ~ 6×10^{-3} m_0c which, in its turn, is close to the magnitude of the Fermi momentum of the electron-positron momentum density distribution, p_F (Fig. 1). Such behaviour of the electron-positron momentum density distribution is characteristic for [110] crystallographic direction of the elemental diamond-like semiconductors where the step-like drop mentioned above indicates the reflection of waves of the bonding electrons at the Jones zone face (see [2, 29, 46] and references therein). Also, we would like to note that the *behavior of calculated total function of the electron-positron momentum density distribution is similar to the experimental momentum distribution* of the annihilation 2γ-

quanta obtained for [110] and [100] crystallographic direction in the diamond-like semiconductors (see, e.g., [29]).

And last (but not the least) concerns the total electron-positron momentum density distributions obtained for different crystallographic directions over the range of 0 to ~ 2.5 $\times 10^{-3}$ $m_0 c$ (this interval corresponds to $\Delta p_z \sim 0 \div 0.33$ *a.u.* in Fig. 1 of Ref. [23] where the anisotropic electron-positron momentum distribution is presented for [110] crystallographic direction of the tetrahedral diamond-like crystal structure of GaAs binary compound). In actual fact, a certain mutual compensation of lower and higher contributions of the partial distributions of calculated electron-positron momentum densities always takes place. Total charge, obviously, is conserved, i.e. the positron wavefunction, obtained after a simple zone-folding, $\Psi_{p,SL}(n=1,\vec{k}=\Gamma_{SL})$ is unchangeable with the accuracy to a constant factor which disappears as a result of integration. Accordingly, the electron-positron total density of states $\Gamma_{SL,total}(\vec{p})$ in the superlattice is compensated by the positively charged ion cores whose total effective charge density is $\rho_{SL.or.Bulk}(\vec{r}) = const.\sum_{occ}\left|\Psi_{SL.or.Bulk}\right|^2$.

In case ACAR spectrum is recorded then the probability of detecting a pair of annihilation quanta with a total momentum p is proportional to the average electron-positron momentum:

$$I(p) \cong \iint \Gamma_{total}(\vec{p}) dp_x dp_y \cong const \int_{\theta}^{p_F} p\,\rho(\vec{p}) dp\,, \qquad (3)$$

where $p \approx \theta \cdot m_0 c \approx p_z$, θ is the angle of detection of a pair of the annihilation quanta, $m_0 c$ is the rest momentum of electron, $I(p)$ is the counting rate of the pairs of the annihilation γ-quanta, and p_z is the module of the projection of the electron-positron momentum onto a certain axis z which is perpendicular to the axis of rotation of the movable detector of the ACAR spectrometer. Equation (3) holds for both bulk materials and their superlattice. Actually, the component of the resulting momentum of the pair of γ-quanta, which is equal to the p_z magnitude of the electron-positron momentum, is detected; it is generally accepted that the long-slit scheme of the angular spectrometer allows one to record so-called one-dimensional (1D) spectrum of ACAR (see, e.g. [2, 3, 29]).

In the binary compounds under study, GaAs and AlAs, the function $\rho(p)$, reconstructed from the ACAR spectra, demonstrates its behavior which is typical for the Fermi distribution near to the Fermi momentum. As seen from Fig. 1, the electron-positron momentum density distribution calculated for GaAs/AlAs superlattice as well as the one reconstructed for GaAs and AlAs single crystals, - they are very close to each other over the range of a narrow interval of changes of the Fermi momentum of the bonding electrons. Of paramount practical importance is that this interval includes the values of the Fermi momentum calculated by IPM approximation, i.e. for the undisturbed Fermi gas of the bonding electrons in the crystal lattice. It should be emphasized also that the numeral value of calculated Fermi momentum (p_F) follows the changes of FWHM of the electron-positron momentum density distribution in passing from AlAs to GaAs and AlAs-GaAs superlattice accepting the magnitudes equal to ~ 6.63×10^{-3} $m_0 c$ and ~ 6.7×10^{-3} $m_0 c$ for AlAs and GaAs, respectively (see Fig. 1).

The results under discussion show a very close similarity between the electron-positron momentum density distributions in the valence band over the range of momenta close to the Fermi level for both the binary semiconductors (AlAs, GaAs) and their GaAs/AlAs superlattice. So long as this heterostructure is fabricated in the form of the thin

film it means that two component layers in the "perfect" structure of the superlattice may be detected reliably provided that both sensitivity and resolution of the positron self-seeking microprobe based on measuring ACAR spectra are tangibly increased. In other words, the solving of problem of reliability of the positron diagnostics of the superlattices of the diamond semiconductors will inevitably require, at least, a considerable improvement of the brightness of the slow positron beam which is one of the main component parts of the whole procedure of the positron probing of thin and ultrathin layers [2].

But even if this problem had been resolved the electron-positron momentum density distribution would not have been much different from the ones predicted for AlAs-GaAs superlattice by principal reasons:. the closeness of the electron-positron momentum density distributions in GaAs and AlAs single crystals imposes a certain natural limitations on the effectiveness of the positron probing of a "perfect" GaAs/AlAs superlattice (see Fig. 1 and Fig. 2 as well as experimental data therein). It means, on the other hand, that a practical non-contact/non-destructive characterization of GaAs/AlAs superlattice would be most effective for non-perfect thin films; we are considering such possibility below.

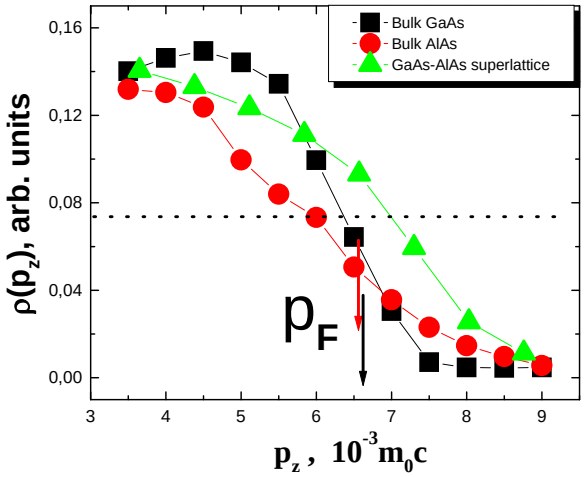

Fig. 1: Total electron-positron momentum density distributions $\rho\ (p_z)$ in the superlattice of GaAs/AlAs calculated for the crystallographic direction [011] (triangles) and the ones reconstructed from ACAR spectra for the constituent materials, AlAs [100] (dots) and GaAs [100] (squares), respectively. The range of momenta ~ $3.5 < p_z < p_F$ is shown to demonstrate *close similarity* of the Fermi distributions of the valence electrons in both GaAs, AlAs single crystals and GaAs/AlAs superlattice under study. Dashed horizontal line is on the level of HWHM of the distributions whose crosses with the spectral lines indicate the change of the Fermi momentum from ~ 6.25 to ~ 6.95 $\times 10^{-3}\ m_0c$ in passing from the diamond-like semiconductors (AlAs and GaAs) to the superlattice GaAs/AlAs, respectively. Upper and lower arrows indicate magnitudes of the Fermi-momenta p_F obtained on the basis of IPM approximation for the valence band of AlAs and GaAs diamond-like semiconductors, respectively; both experimental and calculated p_F magnitudes are very close to each other.

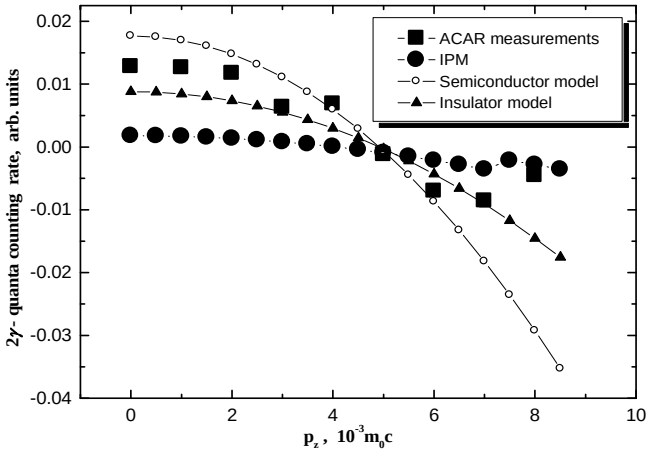

Fig. 2: The difference between the ACAR spectral curves for AlAs and GaAs oriented along the crystallographic direction [111]: squares and dots are experimental and calculated data, respectively. The electron-positron interaction has been neglected, so-called independent particle model, IPM, has been used, see e.g. [36] and references therein; see also text. The electron-positron Coulomb interaction has been taken into account to calculate the difference between the ACAR spectra plotted by the dot-and-line curves: open circles and triangles designate numeral data obtained by so-called semiconductor and insulator models, respectively. *The insulator and semiconductor models demonstrate similar results.* Open circles: $r_s^{\text{eff}} \approx 2.4 a.u$ and $r_s^{\text{eff}} \approx 2.439 a.u$ are the magnitudes of the effective electron density calculated for AlAs and GaAs single crystals, respectively; the magnitudes of r_s^{eff} were taken from Table 2 in Ref. [47]). Triangles: $r_s^{\text{eff}} \approx 2.35 a.u$ and $r_s^{\text{eff}} \approx 2.4375 a.u$ values correspond to AlAs and GaAs binary compounds, respectively (see Table 3 in Ref. [47]).

Of paramount importance is a reliable distinguishing of the ACAR spectra which are generated by the sublattices of GaAs/AlAs superlattice inasmuch as the valence band of the both materials is formed by similar sp^3 - hybridized orbitals. To evaluate qualitatively a magnitude of this similarity, we have calculated the difference between the angular correlation of the 2γ-quanta to be emitted from the valence zone of AlAs and GaAs single crystals, respectively. As a first step, IPM has been used, within the framework of which the thermalized positron was assumed to annihilate in the ideal non-disturbed Fermi-gas of electrons (see above the remarks concerning the insignificance of the enhancement factor in this case). Then a disturbed electron density round the positron has been applied for evaluation both the Fermi momentum and the difference between ACAR curves; and, at last, all difference curves obtained by these ways for AlAs and GaAs single crystals have been compared with experimental data.

The calculations of ACAR have been based on some practical schemes in which the enhancement of the electron density at the positron is supposed to depend on the density (n) of the unperturbed electron gas, $r_s = (3/4\pi n)^{1/3}$ [2, 8, 46]. For [111] crystallographic directions the functions of ACAR are closed to the inverted parabola whose crossing of the abscissa at so-called "cut-off" angle is proportional to the Fermi momentum p_F [2, 29, 46]. To this approximation the difference between ACAR functions is determined, mainly, by the magnitudes of the numeral values of the characteristic electron radius $r_s \approx 13.99 \times p_F^{-1}$ (r_s and p_F are measured in the atomic units and milliradians, respectively [35, 46]). We have estimated this value using the Ferrell's approach in which the numeral value of r_s depends on the ratio of the atomic weight, A, to the specific gravity, d (g/cm^3) [35]:

$$r_s \cong 1.384 \times \sqrt[3]{A/dz}, a.u. \tag{4}$$

where z=4 is the coordination number (or the reduced valence) for the binary A^3B^5 diamond-like semiconductor compounds. As the averaged magnitude of A the half of the molecular weight of the A^3-B^5 molecule has been used [46]. This in itself is a certain approximation, which, however, seems to be quite correct for the calculations of the unperturbed electron densities. Parameter r_s estimated by this way is used to calculate the positron lifetime whose values are in a good agreement with the experimental data available for the diamond-like semiconductors; and, vice versa, r_s values reconstructed by means of the ACAR parameters are very close to the ones estimated by Eq. (4) for unperturbed electron densities for different tetrahedral structures [46]. Accordingly, numeral values of r_s are estimated to be equal to $\approx 2.11 a.u.$ and $\approx 2.081 a.u.$ for AlAs and GaAs, respectively (see Fig. 2).

It is interesting to note in this connection that the electron-positron correlation effects, taken into account within both so-called semiconductor and insulator models, *do not influence considerably on the magnitudes of r_s parameter calculated by Eq. (4)*: for AlAs and GaAs there have been obtained the numeral values $r_s^{\text{eff}} \approx 2.35 \div 2.4 a.u$, and $r_s^{\text{eff}} \approx 2.439 \div 2.375 a.u$, respectively [47]. It takes place owing to relatively low efficiency of the electron-positron correlation effects leading to insignificant increase of enhancement factor of the positron annihilation rate in the electron gas of a rather high electron density, equal to ~ 2.0 *a.u.* [29, 35, 36] (see also above).

Let us estimate how these numeral differences may affect ACAR function calculated for investigated GaAs and AlAs diamond-like semiconductors. One can show that over the range of momenta $0 < p < p_F$ the difference between ACAR spectral curves is given, approximately, by the following simple formula:

$$\Delta I(\theta) \approx B - C \times \theta^2 \tag{5}$$

where $B, C \approx const.$ magnitudes depending indirectly on the effective charges of As atoms in the investigated materials GaAs and AlAs (see [46] and references therein).

As seen from Fig. 2, *a decline* of the difference function of ACAR, calculated by Eq. (5) on the basis of IPM approximation for AlAs and GaAs single crystals, *follows well the experimental data* (compare the data designated by dots and squares in Fig. 2, respectively). The magnitude of the difference shown in Fig. 2 is small: largest discrepancy in the numeral values calculated for these two materials is observed near to the spectral region adjusted to the Fermi momentum (p_F). Having taken into account a roughness of the approximation used, one may consider an agreement between experimental and calculated data as a surprisingly good one (the maximal difference between the curves plotted in Fig. 2 did not exceed ~ 0.55 %).

Of a special attention deserves the *closeness* of this difference of ACAR curves to the one corrected on the basis of the amendments to the electron density around positron caused by the electron-positron Coulomb interaction (see the dot-and-line graphs in Fig. 2): the electron densities obtained by both so-called semiconductor and insulator models [47], respectively, result in the ACAR functions which close to the ones obtained both experimentally and by IPM approximation.

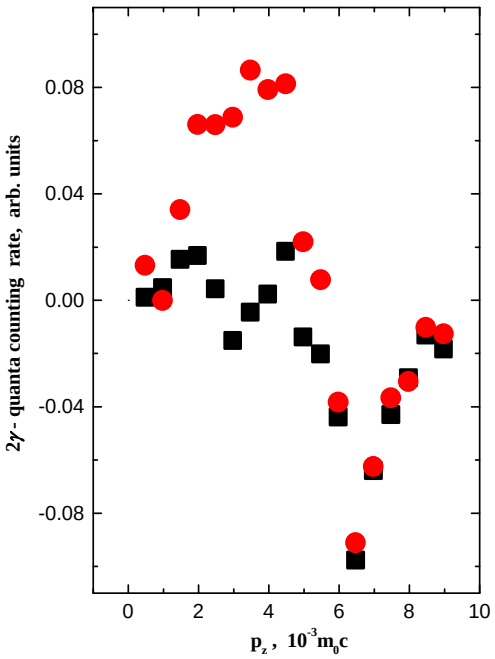

Fig. 3: The difference ACAR curves obtained for AlAs and GaAs single crystals for two cases: 1st – squares: the both crystal lattices of materials are "perfect"; 2nd - dots: AlAs material is "perfect" whereas GaAs crystal lattice contains positron traps which are vacancy-type defects including well-known *EL2* centers (for more detail about these traps see, e.g. [2]). The maximal difference reaches ~ 16 % (shown by arrows to guide the eyes); the error does not exceed tripled diameter of dots.

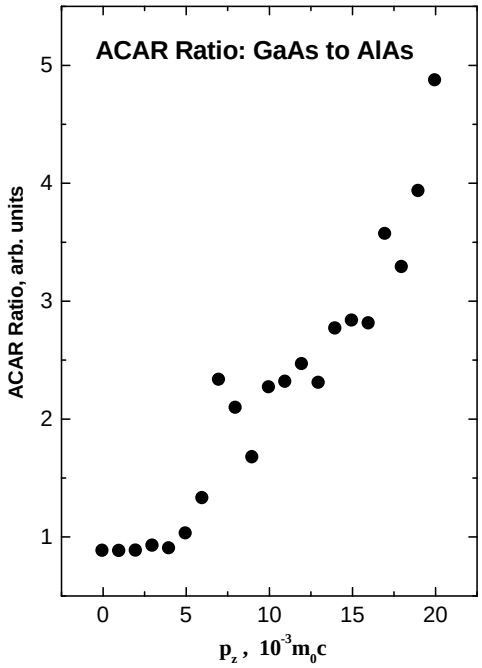

Fig. 4: Ratio of ACAR spectra obtained for parent constituent materials of GaAs/AlAs superlattice: more volumetric cores in GaAs contribute greatly into this ratio over the range of high-momentum component ($p_z \geq 7\times10^{-3}$ m_0c) in contrast to the region of the dominating positron annihilation process with the bonding electrons ($p_z \leq 7\times10^{-3}$ m_0c). We predict that a qualitatively similar effect in the region of high momenta of the annihilation 2γ-quanta should be observed in the measurements performed by the Doppler broadening technique.

Thus, the results of calculations of the electron-positron momentum densities and ACAR curves performed for thin layers of the AlAs-GaAs superlattice as well as for related single crystals of AlAs and GaAs indicate (*i*) smallness of amendments associated with electron-positron Coulomb interactions in the superlattice under study and (*ii*) a necessity of a tangible increase of the sensitivity of the positron particle microprobe when the methods of detection of the electron-positron momentum density distributions are used.

From the viewpoint of a non-destructive/non-contact material characterization this result is quite encouraging because in case of presence of the defects of a vacancy type in one or another sublattices of the superlattice one should expect observing *a marked disturbance* of the electron-positron momentum density distribution which could be detected by determining the properties of the emitted annihilation radiation. As seen from Fig. 3, the difference between ACAR spectra obtained for "perfect" single crystals of AlAs and GaAs (shown by squares) is a little bit less pronounced in comparison with the one obtained in case GaAs single crystal contains the vacancy-type defects (see data designated by dots in Fig. 3). In this case the differences between ACAR spectra should be described in terms of the positron trapping and localization in the free volume related to the vacancy whose environment is decorated by the atoms of a certain elemental specificity.

In this work we have mainly studied GaAs/AlAs heterostructure using both empirical pseudopotential method (EPM) and ACAR technique assuming that the contribution of the ion core electrons is small. Nevertheless, the high-momentum ACAR is, in fact, strongly dependent on the elemental specificity of the ion cores of Ga and Al (see Fig. 4). The observed effect of high difference in the contribution of Ga and Al subvalent electrons into ACAR may pave the way for refining the data obtained by empirical pseudopotential method (EPM) for GaAs/AlAs superlattice.

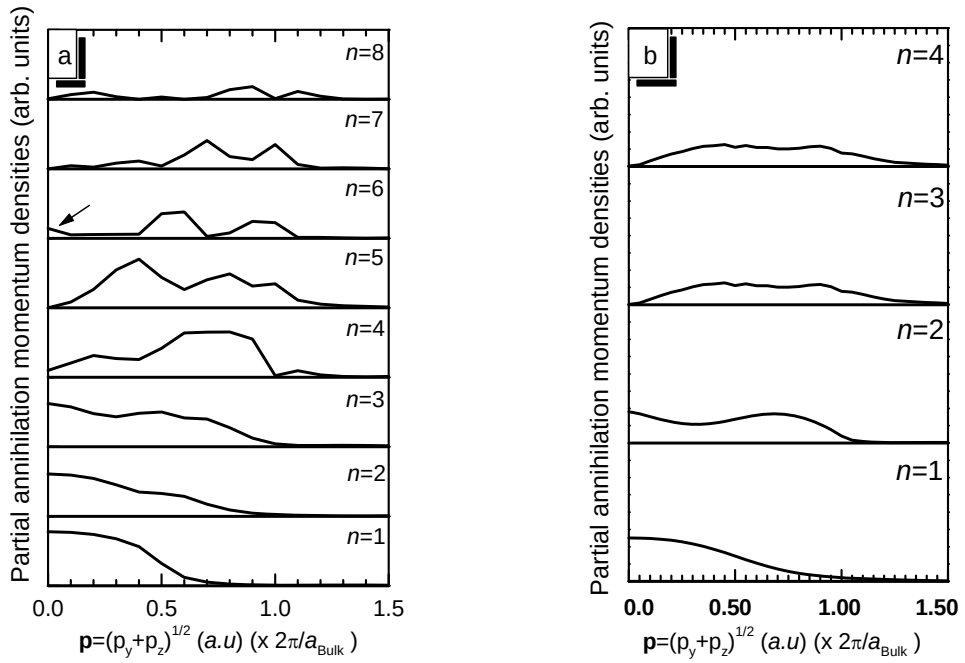

Fig. 5: Partial electron-positron momentum densities calculated for [011] crystallographic direction for (a) eight upper valence bands in $(GaAs)_1/(AlAs)_1$ superlattice, and (b) four upper valence bands in the bulk of GaAs single crystal. In both cases, the index n=1 corresponds to the upper valence band at Γ; n=2 is the band just below at the same point, etc., a_{Bulk} refers to the lattice parameter of GaAs binary compound.

At last, we would like to examine theoretically how, for example, a $(GaAs)_{u=1}/(AlAs)_{v=1}$ superlattice electronic states impact the partial momentum densities: for this purpose we have to compare the calculated data obtained for the superlattice (with the ones obtained for the bulk of GaAs single crystal (see Fig. 5a and Fig. 5b). It is obvious that ACAR technique does not allow one to measure directly the partial electron-positron momentum densities, but the present calculation is interesting not only from the fundamental point of view but it can also be useful for spectroscopic analysis of the total electron-positron momentum density: as an example, see the graphs shown for [011] crystallographic direction in Fig. 1.

In case we consider four valence bands of the bulk, the latter will be "splitted" to eight subbands in the $(GaAs)_1/(AlAs)_1$ and each pair of two successive superlattice valence bands is expected to originate from the folding of one valence band of the host bulk material. In its turn, each pair of the superlattice valence bands will have to have comparable contribution to the annihilation process. This is, however, not always the case because of the mixing that occurs between the valence bands of the GaAs bulk material on which one the superlattice wavefuntion has been expanded. As an example, in Fig. 5a the arrow for the subband n=6 shows clearly a feature which does not exist in the 3rd band of the bulk material of GaAs (Fig. 5b) from which this superlattice subband is expected to be formed (together with the subband n=5). A thermalized positron makes a relatively small contribution to the total momentum of the annihilating pair, and the parameters of the electron-positron momentum distribution are determined by one component of the pair, i.e. by the electron momentum. Therefore, ACAR spectral function reflects, mostly, the anisotropy of the electron momentum density distribution which depends on the direction in the crystal lattice.

5. Conclusion

The merits and demerits of positron non-destructive probing of GaAs/AlAs and its component parts to be used in the heteronanostructures have been considered as the problem of detecting the electron-positron momentum density distribution. The positron states and the electron-positron annihilation in a GaAs/AlAs superlattice have been theoretically calculated and then compared with the experimental data obtained *ad hoc* for GaAs and AlAs single crystals by means of high-precision measurements of the angular correlation of the annihilation radiation (ACAR).

A close proximity of the electron-positron momentum density distributions in AlAs and GaAs crystal lattices, - both in the superlattice under study and the bulk of single crystals, - puts forward a question of a tangible increase of the sensitivity of detecting small (but marked) features of the electron momentum density of the valence band in these chemically related materials. This problem has been emphasized by comparing ACAR spectral functions obtained for the bulk of AlAs and GaAs single crystals. No significant influence of the electron-positron enhancement factor on the electron-positron momentum density in both calculated and experimental electron-positron momentum distributions has been observed. This fact has been taken into consideration when carrying out the calculation of the electron-positron momentum density distributions in GaAs/AlAs superlattice and related materials.

As soon as positron-sensitive traps appear in a tangible concentration, - either in the superlattice or in the relevant bulk materials, - the confinement of the delocalized positron change to a localized state, which is characterized, at least, by considerably different electron-positron momentum density distribution which in itself is a fingerprint of a certain microstructure of the positron trap. The appearance of the defects of a vacancy type (e.g., in

the crystal lattice of GaAs, - as it has taken place in the present work) results in emitting the annihilation radiation characteristic of the localized positrons.

Acknowledgements

We would like to thank the Condensed Matter Section of Abdus Salam International Center for Theoretical Physics for hospitality and financial assistance that made this work possible. We are also especially indebted to Prof. V.E. Kravtsov for discussions and his interest to this research. One of us, N. Yu. A., is grateful to German Academic Exchange Service (DAAD) for financial assistance as well as to Prof. R. Krause-Rehberg and to Dr. V.V. Emtsev for their interest to this work and fruitful discussions. This work has been supported by the ICTP in Trieste, the ENSET of Oran (Algeria), by the Algerian national research projects CNEPRU (J3116/02/05/04, J3116/03/51/05, D05520060007, D05520080001 and D05520100004) and by the Algerian National Project PNR entitled: "Advanced Investigation of Nanostructures (ADIN)", coded "E312/Av05".

References

[1] A. Dupasquier, G. Kögel, A. Somozac, Acta Mater. **52** (2004) 4707
[2] R. Krause-Rehberg, H. S. Leipner, *Positron annihilation in semiconductors: Defect studies*, Springer-Verlag, Ser. In Solid State Physics, **127** (1999) 378
[3] N. Yu. Arutyunov, V. V. Emtsev, Physica B, **401-402** (2007) 609
[4] N. Yu. Arutyunov, V. V. Emtsev, Physica B, **404** (2009) 5128
[5] N. Yu. Arutyunov, V. V. Emtsev, R. Krause-Rehberg, Solid State Phenomena, **156-158** (2010) 455
[6] N. Yu. Arutyunov, V. V. Emtsev, E. Sayed, R. Krause-Rehberg, Solid State Phenomena, **131-133** (2008) 89
[7] N. Yu. Arutyunov, Solid State Phenomena, **69&70** (1999) 333
[8] N. Yu. Arutyunov, R. Krause-Rehberg, Solid State Phenomena, **95-96** (2004) 507
[9] N. Yu. Arutyunov, V. V. Emtsev, Solid State Phenomena, **108-109** (2005) 615
[10] Y. Nagai, M. Hasegawa, Z. Tang, A. Hempel, K. Yubuta, T. Shimamura, Y. Kawazoe, A. Kawai, F. Kano, Phys. Rev. B, **61** (2000) 6574
[11] Y. Nagai, Z. Tang, M. Hasegawa, Radiation Phys. and Chem. **58** (2000) 737
[12] Y. Nagai, T. Chiba, Z. Tang, T. Akahane, T. Kanai, M. Hasegawa, M. Takenaka, and E. Kuramoto, Phys. Rev. Lett. **87** (2001) 176402
[13] Y. Nagai, Z. Tang, M. Hasegawa, T. Kanai, and M. Saneyasu, Phys. Rev. B, **63** (2001) 134110
[14] T. Onitsuka, M. Takenaka, E. Kuramoto, Y. Nagai, M. Hasegawa, Phys. Rev. B, **65** (2001) 012204
[15] M. A. Van Huis, A. Van Veen, H. Schut, C. V. Falub, S. W. H. Eijt, P. E. Mijnarends, J. Kuriplach, Phys. Rev. B, **65** (2002) 085416
[16] Z. Tang, M. Hasegawa, Y. Nagai, M. Saito, Phys. Rev. B, **65** (2002) 195108
[17] Y. Nagai, Z. Tang, H. Ohkubo, K. Takadate, M. Hasegawa, Radiat. Phys. Chem. **68** (2003) 381

[18] A. P. Druzhkov, D. A. Perminov, V. L. Arbuzov, N. N. Stepanova, and N. L. Pechorkina, J. Phys.: Condens. Matter, **16** (2004) 6395
[19] Y. Nagai, T. Toyama, Y. Nishiyama, M. Suzuki, Z. Tang, M. Hasegawa, Appl. Phys. Lett. **87** (2005) 261920
[20] M. Hasegawa, Z. Tang, Y. Nagai, T. Chiba, E. Kuramoto, M. Takenaka, Phil. Mag. **85** (2005) 467
[21] Z. Tang, T. Toyama, Y. Nagai, K. Inoue, Z. Q. Zhu, M. Hasegawa, J. Phys.: Condens. Matter, **20** (2008) 445203
[22] N. Sekkal, H. Aourag, Superlatt. Microstruct. **33** (2003) 63
[23] N. Sekkal, N.Yu. Arutyunov, Physica B, **404** (2009) 5125
[24] Y. Nagai, T. Nonaka, M. Hasegawa, Y. Kobayashi, C. L. Wang, W. Zheng, and C. Zhang, Phys. Rev. B, **60** (1999) 11863
[25] I. Makkonen, A. Snicker, M. J. Puska, J.-M. Mäki, F. Tuomisto, Phys. Rev. B, **82** (2010) 041307 (R)
[26] J. Dekker, R. Aavikko, K. Saarinen, Appl. Surf. Sci. **194** (2002) 97
[27] J. Slotte, K. Saarinen, E.-M. Pavelescu, T. Hakkarainen, M. Pessa, Appl. Phys. Lett. **89** (2006) 061903
[28] J. Slotte, K. Saarinen, E.-M. Pavelescu, T. Hakkarainen, S. Karirinneb, T. Jouhtib, M. Pessab, Physica B, **376-377** (2006) 857
[29] N. Yu. Arutyunov, In: *Condensed matter—new research*, M. P. Das, editor, Nova Science Publishers, New York (2007) 297
[30] See e.g.; M. L. Cohen, and T. K. Bergstresser, Phys. Rev. **141** (1966) 789
[31] L.-W. Wang, and A. Zunger, Phys. Rev. B, **51** (1995) 17398
[32] H. Aourag, B. Khelifa, A. Belaidi, A. Tadjer, M. Rezki, M. Gamoudi, Phys. Stat. Solidi (b), **160** (1990) 193
[33] N. Amrane, Mat. Chem. and Phys. **114** (2009) 283
[34] S. Ishibashi, A. A. Manuel, L. Hoffmann, K. Bechgaard, Phys. Rev. B, **55** (1997) 2048
[35] R. A. Ferrell, Rev. Mod. Phys. **28** (1956) 308
[36] B. Barbiellini, in: *New Directions in Antimatter Chemistry and Physics*, C. M. Surko and F. A. Gianturco, editors, Kluwer Academic Publishers, Netherlands (2001) 127
[37] M. Jaros, K. B. Wong, M. A. Gell, Phys. Rev. B, **31** (1985) 1205
[38] M. A. Gell, D. Ninno, M. Jaros, D. J. Wolford, T. F. Keuch, and J. A. Bradley, Phys. Rev. B, **35** (1987) 1196
[39] M. J. Shaw, Phys. Rev. B, **61** (2000) 5431
[40] M. J. Shaw, M. R. Kitchin, M. Jaros, Phys. Rev. B, **63** (2001) 155303
[41] Ian Morrison, M. Jaros, and K. B. Wong, Phys. Rev. B, **35** (1987) 9693
[42] I. Morrison, L. D. L. Brown, M. Jaros, Phys. Rev. B, **42** (1990) 11818
[43] S. M. North, P. R. Briddon, M. A. Cusack, M. Jaros, Phys. Rev. B, **58** (1998) 12601
[44] M. R. Kitchin, M. Jaros, Physica E, **18** (2003) 498
[45] M. R. Kitchin, Microelectronics Journal, **35** (2004) 461
[46] N. Yu. Arutyunov, Materials Science Forum, **105-110** (1992) 583
[47] M. J. Puska, S. Makinen, M. Manninen, R. M. Nieminen, Phys. Rev. B, **39** (1989) 7666